Applied Surface Science 382 (2016) 80–87

Contents lists available at ScienceDirect

Applied Surface Science

journal homepage: www.elsevier.com/locate/apsusc

A van der Waals DFT study of PtH_2 systems absorbed on pristine and defective graphene

Ignacio López-Corral[a,b], Sebastián Piriz[c,d], Ricardo Faccio[c,d], Alfredo Juan[e,f,*], Marcelo Avena[a,b]

[a] Instituto de Química del Sur (INQUISUR), UNS-CONICET, Av. Alem 1253, B8000 Bahía Blanca, Argentina
[b] Departamento de Química, Universidad Nacional del Sur, Av. Alem 1253, B8000 Bahía Blanca, Argentina
[c] Centro NanoMat/DETEMA, Facultad de Química, Universidad de la República, Montevideo, Uruguay
[d] Centro Interdisciplinario de Nanotecnología, Química y Física de Materiales (CINQUIFIMA), Facultad de Química, Universidad de la República, Montevideo, Uruguay
[e] Instituto de Física del Sur (IFISUR), UNS-CONICET, Av. Alem 1253, B8000 Bahía Blanca, Argentina
[f] Departamento de Física, Universidad Nacional del Sur, Av. Alem 1253, B8000 Bahía Blanca, Argentina

ARTICLE INFO

Article history:
Received 27 November 2015
Received in revised form 10 February 2016
Accepted 8 April 2016
Available online 11 April 2016

Keywords:
Graphene
van der Waals
Hydrogen storage
Kubas

ABSTRACT

We used a density functional that incorporates van der Waals interactions to study hydrogen adsorption onto Pt atoms attached to carbon-vacancies on graphene layers, considering molecular and dissociated hydrogen-platinum coordination structures. PtH_2 complexes adsorbed on several sites of pristine graphene were also studied for comparison. Our results indicate that both a Kubas-type dihydrogen complex and a classic hydride without H—H bond are the preferential PtH_2 systems on the vacancy site of graphene. In contrast, the Kubas complex is unstable onto pristine graphene and the hydride is obtained at all adsorption sites. Our simulations suggest that the C-vacancy decreases the reactivity of the metal decoration, allowing a non-dissociative hydrogen adsorption. The H_2 molecule is oriented almost perpendicular to the outermost C—Pt bond, interacting also with the graphene surface through σ-H and π-C states. This stabilization of the Kubas-type complex could play a very important role for hydrogen storage in Pt-decorated carbon adsorbents with vacancies.

1. Introduction

Hydrogen is a versatile and nontoxic energy carrier, but an effective and stable storage medium is still the major barrier in the development of hydrogen-based technologies. In recent years, several categories of solid systems have been studied to satisfy the US Department of Energy (DOE) hydrogen storage targets for light-duty vehicles. Transition metal hydrides and light metal hydrides are good candidates, but these systems have high weight and high activation barriers for both adsorption and desorption. The stability is another problem in light hydrides [1]. Recently, attention has been focussed on carbon nanostructures, which have been regarded as potential materials for storing hydrogen safely and efficiently. However, many theoretical and experimental studies have shown that the interaction energies between physisorbed hydrogen molecules and bare nanocarbons are very low at ambient conditions [2]. Due to the weak interaction, the hydrogen storage targets for transport applications cannot be reached using pristine carbon based substrates.

A possible method of increasing the interaction energy is by incorporating transition metal atoms. The enhanced storage capacity has been attributed to different mechanisms, which can occur in parallel: hydride formation in metal nanoparticles, spillover and Kubas-type bonding. The spillover process involves the dissociation of the hydrogen molecule on the metallic decoration [3], while Kubas bonding is based on multiple σ-bonding between dihydrogen molecules and *d* orbitals of transition metal atoms [4]. In a recent work, Contescu et al. [5,6] performed atomic resolution aberration-corrected scanning transmission electron microscopy observations and quantum mechanical calculations of hydrogen adsorbed on activated carbon fibers decorated with palladium nanoparticles, with an 18 wt% of the total Pd content dispersed as single atoms throughout the carbon matrix. Their results suggest that spillover dominates at high pressures, while Kubas-type bonding has increasing contribution at low and medium pressures. In this way, the complexation mechanism could play a very important

* Corresponding author.
E-mail address: cajuan@uns.edu.ar (A. Juan).

http://dx.doi.org/10.1016/j.apsusc.2016.04.057
0169-4332/

role in the hydrogen uptake when carbon materials are decorated with highly dispersed metal nanoparticles. First principles calculations propose that Kubas complexes can be originated when hydrogen is adsorbed on carbon systems decorated with transition metal atoms such as Pd, Ni and Fe [7,8], but H_2 dissociates spontaneously on carbon-supported Pt and Ru [9,10].

In particular, graphene presents some advantages as material for hydrogen storage devices, like extremely high specific surface area, robustness, mechanical flexibility, low weight and efficient binding of hydrogen atoms because of the change in hybridization of carbon atoms from sp^2 to sp^3 [11]. Both transition metal decoration and chemical functionalization of graphene have been proposed to enhance the hydrogen adsorption under ambient conditions [12]. These modified graphenes have better properties as storage medium for hydrogen compared to other porous solid adsorbents. For example, the H_2 uptake capacities in graphene-like materials are typically between 1 and 4 wt% at 300 K, while metal-organic frameworks, zeolites or nanostructured carbons exhibit a maximum of up to 1 wt% [13]. Moreover, the heat of H_2 adsorption in functionalizated graphenes is mostly between 8 and 15 kJ/mol, much higher than that in other porous carbons (4–6 kJ/mol) [13].

However, metal atoms adsorbed on pristine graphene have a tendency to form clusters because the cohesive energy of the metal is stronger than the carbon-metal binding and there are no kinetic barriers opposing surface diffusion. Clustering decreases the effectiveness of metal doping on the hydrogen storage capacity [14,15], and can change the storage mechanism from Kubas-type complexation to chemisorptive dissociation. This process can be moderated by stabilizing the metal atoms on the carbon surface by means of different methods, including chemically doped graphene [16,17], porous graphene [18], graphene oxide [19] and carbon vacancies [20–22]. In particular, the presence of vacancies leads to a considerable increase in the adsorption energy of metal atoms on carbon nanomaterials, preventing the clustering phenomenon, so metal-vacancy complexes can be active hydrogen adsorption sites to be used for hydrogen storage. Recently, metal decoration and defect engineering have been proposed in graphene to improve this hydrogen storage capacity. Previous theoretical studies about multiple H_2 adsorption on metal-doped defective graphenes [23–25] report storage capacities close to the target of 6 wt% specified by US DOE for commercial applications, with binding energy values adequate for reversible storage at ambient temperature, between −0.2 and −0.7 eV/H_2.

In this report we applied ab-initio methods with dispersion corrections to investigate the adsorption of hydrogen on Pt atoms anchored to vacancies in graphene, taking into account Kubas complexes and other coordination structures. Taking into consideration that experimentally it is probable to have multiple vacancies in real graphite and graphene samples [26,27], we think that these defects could be used for pinning and passivation of Pt atoms, with potential applications in hydrogen storage. Our aim is to guide new experiments in order to confirm our findings, paying more attention to interactions between defects and transition metals on graphene.

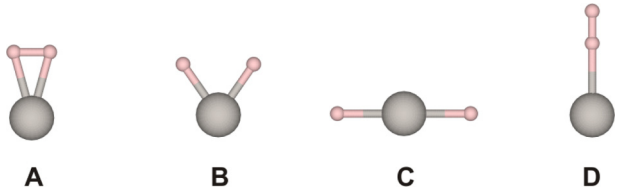

Fig. 1. Initial geometries for H_2 interacting with a free Pt atom. The pink and grey balls correspond to hydrogen and platinum atoms, respectively. (For interpretation of the references to colour in this figure legend, the reader is referred to the web version of this article.)

2. Computational

Density Functional Theory (DFT) calculations [28,29] were performed for the study of structural and electronic properties for Pt-decorated graphene sheets using the projector-augmented wave (PAW) method [30,31] as implemented in the Vienna ab initio simulation package VASP [32]. An energy cutoff of 500 eV was used to expand the Kohn-Sham orbitals into plane wave basis sets. In addition to the 5*d* and 6*s* valence states, the 5*p* semicore states of Pt have been explicitly treated as valence states throughout this work. In all of the calculations reported here, van der Waals (vdW) interactions were incorporated through the vdW-DF functional [33–35], which adds a correction to the generalized gradient approximation (GGA) exchange-correlation (XC) functional. A Monkhorst-Pack *k*-point mesh [36] equivalent to $4 \times 4 \times 1$ was taken for the full (reducible) Brillouin Zone, allowing the convergence of total energy and forces.

We modeled the graphene surfaces using a (5×5) supercell. On this basis, we considered several configurations: pristine graphene (g55), defective graphene (g55v), Pt-decorated graphene (Pt-g55) and Pt-doped defective graphene (Pt-g55v) with a single carbon atom vacancy. In all the cases the vacuum distance was ∼20 Å, in order to avoid the interaction among images in adjacent cells. Both supercell dimensions and ions positions were allowed to optimize, until residual forces and stress tensor components were positioned down to 0.01 eV/Å and 5 kbar respectively.

We further performed overlap population (OP) analysis [37] using the SIESTA [38,39] code to study the evolution of chemical bonding. We selected the standard double-ξ basis set with polarization orbitals (DZP) [40] and the vdW-DF functional [33,34]. The real-space grid used to represent the charge density and wave functions was the equivalent of that obtained from a plane-wave cutoff of 400 Ry, and the Brillouin-Zone sampling was up to $10 \times 10 \times 1$.

It is well known that DFT suffers from static and dynamic correlation errors and may not be appropriate for transition metals. However, several recent publications employed this methodology [22,41–43]. In our case, we emphasize in the discussion of the relative stability of the different PtH_2 complexes, so we think a DFT approach is suitable for this purpose.

3. Results and discussion

3.1. Isolated PtH_2 systems

We started considering the interaction of an isolated Pt atom with hydrogen. The interactions can be classified in four geometries: the free Kubas complex (A), hydride without H—H bond (B), linear H—Pt—H hydride (C) and the free terminal H—H···Pt dihydrogen complex (D). The corresponding geometries and sketches are presented in Table 1 and Fig. 1. The binding energy (*BE*) is determined as: $BE(H_2) = E(PtH_2) - E(H_2) - E(Pt)$, where $E(PtH_2)$ corresponds to one of the A, B, C or D system, $E(H_2)$ is the energy of

Table 1
Binding energies (BE), magnetic moments (μ), Pt—H and H—H distances for PtH_2 systems.

PtH_2 system	BE (eV)	$\mu(\mu_B)$	d_{Pt-H} (Å)	d_{H-H} (Å)
A	unstable	–	–	–
B	−2.61	0	1.53	2.12
C	−0.10	1.383	1.67	–
D	−0.43	0	1.74	0.81

$BE(H_2) = E(PtH_2) - E(H_2) - E(Pt)$

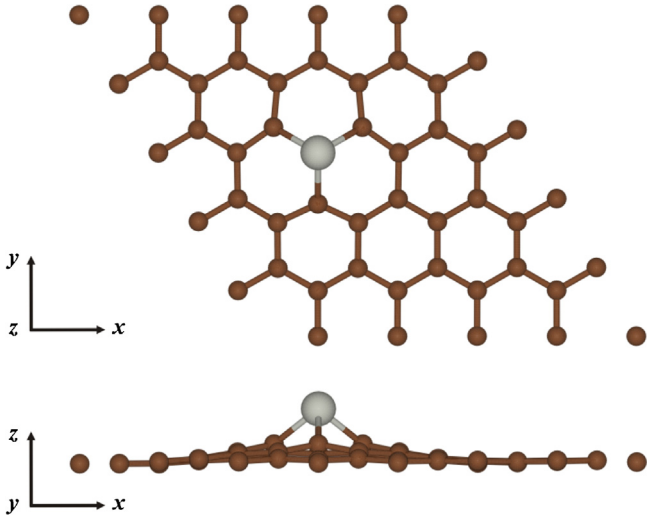

Fig. 2. Final geometry for Pt sited on the vacancy for g55v. The grey and brown balls correspond to platinum and carbon atoms, respectively. (For interpretation of the references to colour in this figure legend, the reader is referred to the web version of this article.)

free H_2 molecule and E(Pt) is the energy of free Pt atom. We based all the initial geometries on the Kubas complexes.

The results suggest that complex A is not stable and changes to complex B, which is actually the most stable free PtH_2 configuration. Isolated Pt is very reactive and easily weakens the H—H bond, leading to a situation that can be considered as a hydride. This is the reason why complex A is unstable and conducts to the isomer B. In the same way, Dag et al. [44] found by means of GGA-DFT calculations that a single H_2 molecule dissociates on a free Pt atom, with final Pt—H and H—H distances of 1.51 Å and 2.08 Å, respectively. On the contrary, Kubas complex is the most stable coordination structure in the case of isolated PdH_2 systems [7]. PtH_2 isomer D is energetically favorable, but presents long-range dispersion forces between Pt and H atoms. Finally, the linear system C has longer Pt—H bonds and becomes the less stable free geometry. Results suggest that complex B can be considered as a mixed situation in which the H—H bond is remarkably elongated, conducting to an intermediate configuration much more stable between $H_2\cdots$Pt aduct (complex A) and linear hydride (complex C). When the H_2 molecule is broken and complex C is originated, the ground state of the system is a triplet. The magnetic moment at Pt is 1 and the remaining magnetic moment is shared with the H atoms by sigmas bonding. Moreover, when forcing complex C to a single state, we noted that the complex is less stable than triplet by 0.45 eV.

3.2. Interacting Pt/graphene systems: Pt-g55 and Pt-g55v

We next considered the interaction of a single Pt atom with pristine (g55) and defective (g55v) graphene. In the first case we explored the three well known adsorption sites: bridge (above a C—C bond), hollow (above a C_6 hexagon) and top (above a C atom). For defective graphene there is only one case, where Pt atom is sited on the monovacancy. Table 2 resumes the energetic and structural properties of these systems. The binding energy is determined as: BE(Pt) = E(Pt/g55) − E(Pt) − E(g55), where E(Pt/g55) corresponds to the non-defective graphene with a Pt atom adsorbed on the bridge/top/hollow site, E(Pt) is the energy of free Pt atom and E(g55) is the energy of isolated pristine graphene. In the case of defective graphene, the binding energy is determined as: BE(Pt) = E(Pt/g55v) − E(Pt) − E(g55v), where E(Pt/g55v) is the defective graphene with a Pt atom adsorbed on the vacancy and E(g55v) is the energy of isolated graphene with a vacancy. We also determined the formation energy of the monovacancy (FE) by means of the following expression [45]: FE(v) = E(Pt/g55v) − E(Pt) − N(g55v) μ(C), where μ(C) corresponds to the chemical potential for carbon and N(g55v) indicates the total number of carbon atoms in the defective system. The chemical potential for graphene was determined as in Ref. [45] as the energy per atom in the case of pristine material: μ(C) = E(g55)/N(g55), where N(g55) is the total number of carbon atoms in non-defective graphene.

Table 2
Binding energies (BE), C—Pt and C—C distances for Pt-g55 and Pt-g55v systems. For C—C bonds, first-neighbor interactions are indicated.

System	BE (eV)	d_{C-Pt} (Å)	d_{C-C} (Å)
Pt-g55 bridge	−1.26 eV	2 × 2.15	1 × 1.47
Pt-g55 top	−1.13 eV	1 × 2.07	3 × 1.46
Pt-g55 hollow	−0.47 eV	6 × 2.41	6 × 1.44
Pt-g55v	−8.51 eV	3 × 1.96	3 × 1.41
BE(Pt) = E(Pt/g55) − E(Pt) − E(g55)			
BE(Pt) = E(Pt/g55v) − E(Pt) − E(g55v)			

Table 3
Binding energies (BE), Pt—H, H—H and C—Pt distances for H_2(B/D)Pt-g55 systems (hollow/bridge/top).

System	BE (eV)	d_{Pt-H} (Å)	d_{H-H} (Å)	d_{C-Pt} (Å)
H_2(B)Pt-g55 bridge	−1.91	2 × 1.55	1 × 1.89	2 × 2.55
H_2(B)Pt-g55 top	−2.04	2 × 1.55	1 × 1.88	1 × 2.45
H_2(B)Pt-g55 hollow	−2.62	2 × 1.55	1 × 1.95	6 × 2.72
H_2(D)Pt-g55 bridge	−0.60	1 × 1.86	1 × 0.75	2 × 2.18
H_2(D)Pt-g55 top	−0.61	1 × 1.85	1 × 0.75	1 × 2.12
H_2(D)Pt-g55 hollow	−0.77	1 × 1.77	1 × 0.77	6 × 2.55
$BE(H_2)$ = $E(H_2/Pt/g55) - E(H_2) - E$(Pt/g55)				

According to these results, there is a reasonable interaction between Pt and g55, being the bridge position the most stable configuration with a binding energy of −1.26 eV. The following configuration in order of stability corresponds to top, with a BE = −1.13 eV. This behavior is expected on the basis of the number of formed C—Pt bonds: two new C—Pt bonds are originated when the Pt atom is absorbed at the bridge site, but only one C—Pt bond is present at the top site. Finally, the less stable configuration corresponds to the hollow geometry, where the electron density in graphene is lower than at the bridge and top sites, with BE = −0.47 eV. Table 2 reveals that there is an enhancement in the C—Pt distance with the coordination of the Pt atom, from the top over the bridge to the hollow site. On the other hand, a trend similar to that for the stability of the adsorption sites (hollow < top < bridge) is found for the neighboring C—C bonds right below the decoration, indicating a stronger interaction of the Pt adatom at the bridge site on pristine graphene. Recent DFT calculations without dispersion forces indicate that the bridge site is the energetically the most favorable for Pt atom adsorption on non-defective graphene sheets, with BE = −1.60 eV and d_{C-Pt} = 2.11 Å [46]. In agreement, we obtain BE = −1.57 eV and d_{C-Pt} = 2.10 Å for the g55-Pt-bridge system when the GGA method is used, so vdW corrections introduce an elongation of the C—Pt bond of about 2.3%. Our results are consistent with previous DFT studies on Pt-functionalized pristine graphene [47–49].

In the case of Pt interacting with defective graphene g55v the situation is clearly different. As can be observed from Table 2, the interaction between Pt and the carbon vacancy is highly exothermic, due to the unsaturated d-shells of Pt adatoms can form strong covalent bonds with the under-coordinated C atoms [49]. In this way, the Pt atom will occupy a vacancy site in preference to a pristine surface site. Notice that the energy of the Pt–vacancy interaction is greater than the cohesive energy of Pt (5.84 eV/atom [50]), so we could assume that the presence of vacancies may help to reduce clustering of platinum on the graphene layer. It can be seen

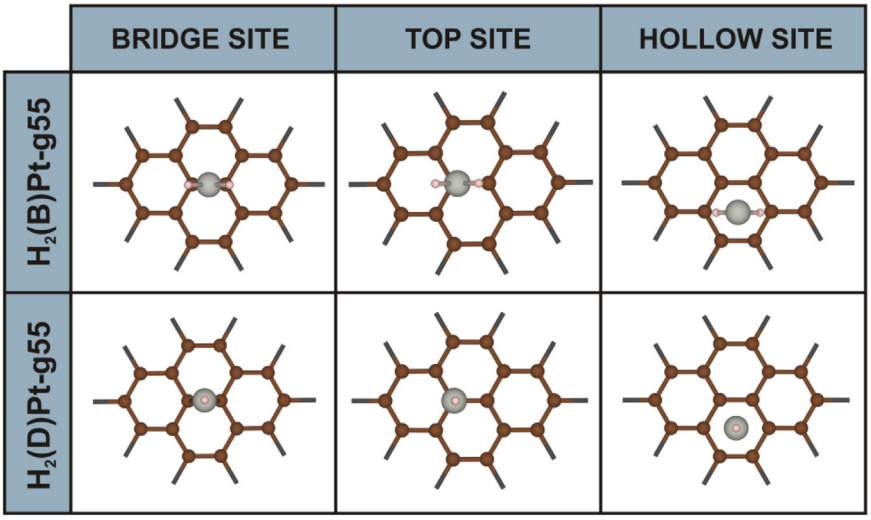

Fig. 3. Final geometries of PtH_2 systems with Pt located on bridge, hollow and top position in reference to graphene layer. The pink, grey and brown balls correspond to hydrogen, platinum and carbon atoms, respectively. (For interpretation of the references to colour in this figure legend, the reader is referred to the web version of this article.)

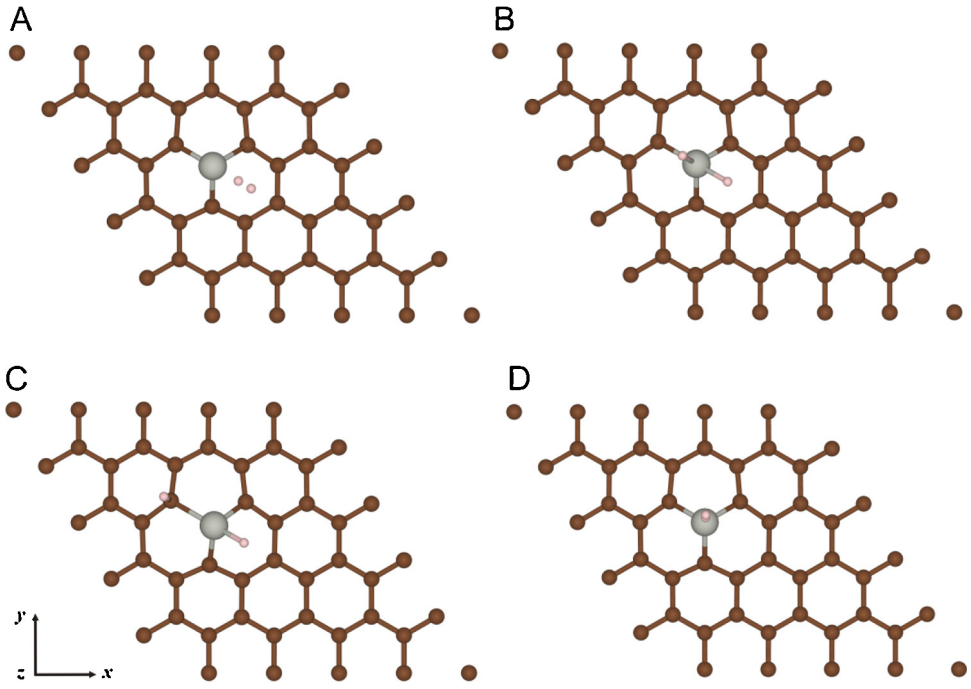

Fig. 4. Final geometries of H_2(A/B/C/D)Pt-g55v interactions. The pink, grey and brown balls correspond to hydrogen, platinum and carbon atoms, respectively. (For interpretation of the references to colour in this figure legend, the reader is referred to the web version of this article.)

from Fig. 2, the Pt atom is moved away from the carbon layer, with a final C—Pt bond length of 1.96 Å, in agreement with literature results [51]. We also found that the formation of the monovacancy requires 1.08 eV.

3.3. H_2 adsorption over Pt-g55

In principle, we have three different adsorption sites for Pt on pristine graphene, corresponding to bridge, top and hollow configuration. Starting from these configurations, we generated for each one of them four possible H_2 adsorption geometries, according to Kubas complex A, hydride B, linear hydride C and linear $H_2\cdots$Pt complex D. The binding energies were determined as: $BE(H_2) = E(H_2/Pt/g55) - E(H_2) - E(Pt/g55)$, where $E(H_2/Pt/g55)$ corresponds to the hydrogen molecule adsorbed on the Pt-decorated pristine graphene, $E(H_2)$ is the energy of free H_2 molecule and $E(Pt/g55)$ is the energy of non-defective graphene with a Pt atom on the bridge/top/hollow site.

In all the cases, we found that the Kubas complex H_2(A)Pt-g55 is unstable and the hydride H_2(B)Pt-g55 is obtained. Similarly, the linear hydride H_2(C)Pt-g55 is unstable at all the configurations, obtaining again the hydride complex H_2(B)Pt-g55. Therefore, the only two stable PtH_2 configurations on pristine graphene correspond to the hydride and the dihydrogen complex. Table 3 presents the binding energies, Pt—H, H—H and C—Pt distances for H_2(B/D)Pt-g55-hollow, H_2(B/D)Pt-g55-bridge and H_2(B/D)Pt-g55-top configurations, as shown in Fig. 3. The projected magnetic

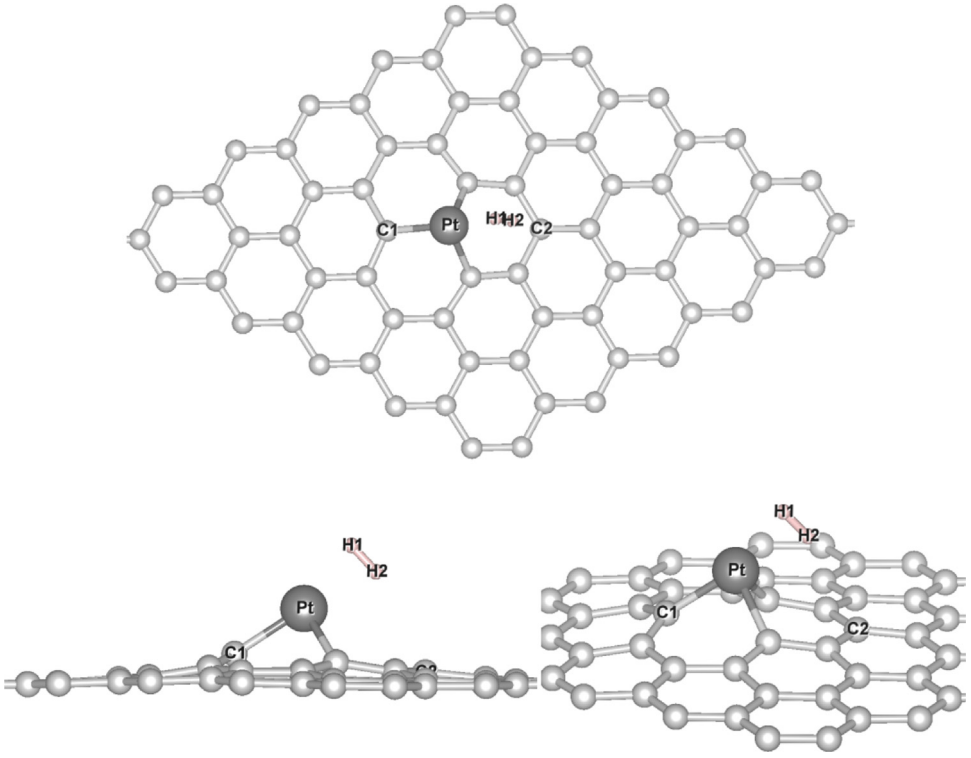

Fig. 5. Three views of the final geometry for H_2(A)-Pt-g55v system. Note the almost perpendicular orientation of H_2 molecule to the C(1)—Pt bond.

moment for each Pt atom in PtH_2 complexes adsorbed on pristine graphene was found equal to zero in all cases.

As can be observed, the most stable configuration corresponds to H_2(B)Pt-g55-hollow with a $BE = -2.62$ eV. In this case, the H—H distance is decreased 7.8% with respect to the value obtained in the unsupported hydride complex PtH_2(B), while the Pt—H distance is elongated 1.0%. The energetic stability is followed by the other two hydrides, H_2(B)Pt-g55-top and H_2(B)Pt-g55-bridge, with $BE = -2.04$ eV and -1.91 eV respectively. The reason of the stability of H_2(B)Pt-g55-hollow structure could be explained in terms of the weaker C—Pt interactions developed in the hollow configuration, as early mentioned in the preceding section. In the same way, the Pt-g55-bridge system, which is the more stable Pt-g55 geometry, is less favored for H_2 adsorption. The bond length of H—H in H_2(B)Pt-g55-top and H_2(B)Pt-g55-bridge systems are shorter than that of H_2(B)Pt-g55-hollow configuration. It can also be seen in Table 3 that CPt distances are elongated after H_2 adsorption on the decoration for the three H_2(B)Pt-g55 complexes (compare with C—Pt lengths for the Pt-g55v system in Table 2). Our geometrical parameters for the H_2(B)Pt-g55-hollow and bridge systems are in good agreement with those reported by Dag et al. [44], who also found that the hollow configuration leads to relatively weaker interaction between Pt and carbon surface and stronger interaction between H_2 and Pt.

Similar considerations can be made when considering the dihydrogen complex H_2(D)Pt-g55. The same trend $BE_{hollow} < BE_{top} < BE_{bridge}$ is observed, but this type of interaction is considerably lower in energy than that of conventional hydrides, approximately by a factor of three. Table 3 shows that the H—H bond in the H_2(D)Pt-g55 systems is lengthened up to 3.6% with respect to the distance in the complex PtH_2(D) in vacuum. At the same time, the Pt—H bond for the hollow geometry is 5.4 and 4.6% shorter than those belonging to the top and bridge configurations, respectively, where the interactions between H_2 and Pt are weaker. As in the graphene-supported PtH_2(B) complexes, C—Pt distances of the Pt-g55 systems are elongated after hydrogen adsorption in the H_2(D) mode interaction.

Table 4
Binging energies (BE), Pt—H, H—H and C—Pt distances for H_2(A/B/C/D)Pt-g55v systems.

System	*BE* (eV)	d_{Pt-H} (Å)	d_{H-H} (Å)	d_{C-Pt} (Å)
H_2(A)Pt-g55v	−0.42	1 × 1.86 1 × 1.90	1 × 0.84	2 × 1.99 1 × 1.95
H_2(B)Pt-g55v	−0.50	2 × 1.66	1 × 2.14	2 × 1.99 1 × 2.04
H_2(C)Pt-g55v	−0.11	1 × 1.67 1 × 2.27	–	2 × 1.97 1 × 2.12
H_2(D)Pt-g55v	−0.41	3.39	1 × 0.74	3 × 1.96

$BE(H_2) = E(H_2/Pt/g55\,v) - E(H_2) - E(Pt/g55\,v)$

3.4. H_2 adsorption over Pt-g55v

As mentioned before, the interaction of a single atom vacancy on graphene with Pt leads to only one structure. For this reason we just evaluated the different coordination geometries for H_2: A–D. Detail overlap population (OP) analysis was addressed for all H_2-Pt-g55v systems. Results are listed in Table 4 and final geometries are shown in Fig. 4. The binding energies were determined as: $BE(H_2) = E(H_2/Pt/g55v) - E(H_2) - E(Pt/g55v)$, where $E(H_2/Pt/g55v)$ corresponds to the hydrogen molecule adsorbed on the Pt-decorated defective graphene, $E(H_2)$ is the energy of free H_2 molecule and $E(Pt/g55v)$ is the energy of defective graphene with a Pt atom on the vacancy site. We found that the magnetic moment at Pt was zero in all g55v-adsorbed complexes.

In this situation the most stable coordination structures correspond to PtH_2 A, B and D complexes, in difference of what was observed in the previous cases. The H—H distance is elongated from 0.74 Å to 0.84 Å during hydrogen adsorption in the Kubas-type mode, with a $BE = -0.42$ eV. The corresponding OP value decreased to 0.438 (from 0.484 for free dihydrogen), indicating a significant

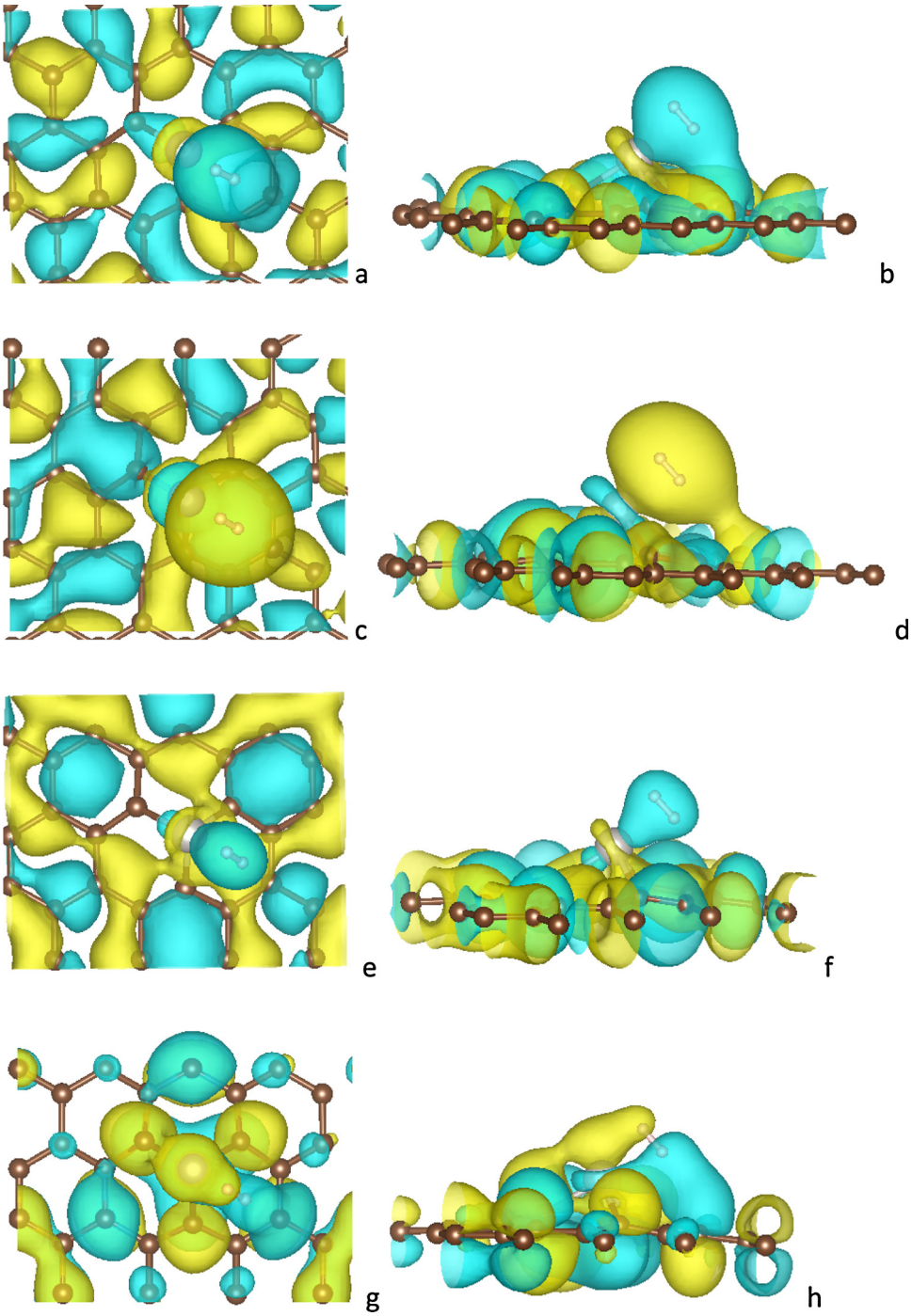

Fig. 6. Two different projections for charge density associated to the individual eigenvalues, and thus for individual monoelectronic wavefunctions, plotted at Γ-point. The eigenvalues were selected because their contribution from hydrogen states. 6a to f correspond to occupied states and 6g to h to unoccupied states.

weakening without bond breaking. Relatively weak Pd—H bonds are developed in this configuration, with a length up to 1.90 Å and an OP value of 0.112. Simultaneously, the three C—Pt bonds are affected after H_2 adsorption: two bonds are elongated 1.6%, with an OP reduction to 0.302 from 0.324 in Pt-g55v, while the other C—Pd bond is shortened 0.9%, with a strengthening of 18.2%.

The hydride complex H_2(B)-Pt-g55v, with a $BE = -0.50$ eV, is a little more stable that the A complex. However, in this case the H—H distance is elongated to 2.14 Å, with a zero overlap population. These findings are in agreement with results obtained by Park et al. [52], who found that the H_2 molecule is dissociated on a single Pt atom adsorbed on the monovacancy of a carbon nanotube, with a final H—H distance equal to 2.16 Å. The Pd—H bonds, which have a length of 1.66 Å, result stronger than those in the A complex, with OP values up to 0.306. Two C—Pt overlaps are stretched 1.6% and weakened 4.3% when the hydride structure is originated, while the remaining C—Pt bond is elongated to a great extent, involving a weakening of about 0.6%. While both H_2(A/B)-Pt-g55v systems are quite close in energy, it is important to mention that activation energies could influence on the possibility to obtain both complex in a real system.

The another adsorbed dihydrogen coordination structure, H_2(D)-Pt-g55v, is very close in energy to the A system, with a $BE = -0.41$ eV. However, a smaller *BE* value is obtained when vdW

corrections are not included, so we can assume that non-local dispersion forces are the main responsible for interaction of molecular hydrogen with Pt-g55v in this bonding configuration. A long Pt—H distance is obtained in this case, with a null overlap. In agreement, the length and OP values of C—Pt and H—H bonds are very similar to those belonging respectively to Pt-g55v and free H_2, thus indicating a moderate interaction between these two fragments.

Finally, in the case of the linear hydride H_2(C)-Pt-g55v, the obtained *BE* (−0.11 eV) indicates a considerable low interaction. As it can be seen in Fig. 4, after generation of PtH_2(C) complex on the monovacancy it is possible to obtain H atoms interacting with graphene, producing a C—H bond with a length of 1.13 Å and a very important OP value (0.528). Only one significant Pt—H overlap is achieved in this situation, with a bond distance of 1.67 Å and an OP of 0.331. C—Pt interactions are also affected: two bonds undergo an elongation of only 0.5%, with a decrease in their OP values of 5.2%, but the other bond results considerably stretched (8.0%) and weakened (34.3%) after adsorption.

All these results are relevant, because Kubas-type complex allow us to retain H_2 molecules without bond breaking. We decided to achieve further tests, in order to explain the origin of the energetic stabilization. The first test consisted in performing the same type of calculation but in a (6 × 6) graphene supercell (g66v), obtaining in this case a *BE* = −0.43 eV, almost identical to the *BE* = −0.42 eV for g55v. Small differences in geometry were found. This test confirms that supercell size is adequate for describing *BE* and geometrical parameters too. Another relevant point consists in the particular orientation of the H_2 molecule in the A complex. Fig. 5 shows that the H_2 molecule is orientated almost perpendicular to the C(1)—Pt bond, where C(1) corresponds to the outermost carbon atom in the graphene layer. We considered several initial configurations for complex A, but after optimization all of them converge to the same final geometry, as presented in Fig. 5.

Finally, we selected the energy regions from the density of states of the H_2(A)-Pt-g55v system in which there are important contributions from hydrogen states. After this, we selected the eigenvalues for those energy regions and we plotted the charge density associated to the individual eigenvalues, and thus individual mono-electronic wavefunctions were evaluated at Γ-point. The plots were carried out using the VESTA software package [53]. Fig. 6 presents four different individual monoelectronic wavefunctions, three from occupied states (Fig. 6a–f) and one from unoccupied states (Fig. 6g and h), in which is it evident the contribution from H atoms. From this information is it possible to understand the particular orientation of the Kubas complex, where the H_2 molecule interacts with Pt and one carbon atom from graphene, C(2) from Fig. 5. This interaction can be considered between a σ-H and π-C states. It is noteworthy that the interaction is not sufficient to weak the H—H bond, since it still can be considered as a Kubas complex. The strong Pt-graphene interaction reduces the reactivity of the free metal atom, and at the same time graphene offers an additional weak interaction with the H_2 molecule, which enables an stabilization without an important weakening the H—H bond.

4. Conclusions

We evaluated by GGA-vdW methods the interaction of hydrogen molecule with Pt-decorated graphene at vacancy sites. The role of graphene is very important, since it enables the reduction in the reactivity of the free Pt atom and at the same time provides an interaction with the H_2 molecule towards the formation of a Kubas-type complex. According to the results, single carbon vacancies passivated with individual Pt atoms could provide an interesting system for hydrogen storage. Multiple H_2 adsorption on Pt-doped graphene with defects will be the subject of a further investigation.

Acknowledgments

ILC, AJ and MA are researchers of CONICET and acknowledge the financial support of SGCyT-UNS, ANPCyT (PICT 2014-1351), CONICET (PIP 2014-2016:11220130100436CO) and FONCyT (Argentina). SP and RF wish to thank the Uruguayan funding institutions: CSIC, ANII and PEDECIBA.

References

[1] L. Schlapbach, A. Zuttel, Nature 414 (2001) 353.
[2] P. Jena, Materials for hydrogen storage: past, present, and future, J. Phys. Chem. Lett. 2 (2011) 206–211.
[3] R.T. Yang, Y. Wang, Catalyzed hydrogen spillover for hydrogen storage, J. Am. Chem. Soc. 131 (2009) 4224–4226.
[4] G.J. Kubas, Molecular hydrogen complexes: coordination of a σ bond to transition metals, Acc. Chem. Res. 21 (1988) 120–128.
[5] C.I. Contescu, K. Van Benthem, S. Li, C.S. Bonifacio, S.J. Pennycook, P. Jena, N.C. Gallego, Single Pd atoms in activated carbon fibers and their contribution to hydrogen storage, Carbon 49 (2011) 4050–4058.
[6] K. Van Benthem, C.S. Bonifacio, C.I. Contescu, N.C. Gallego, S.J. Pennycook, STEM imaging of single Pd atoms in activated carbon fibers considered for hydrogen storage, Carbon 49 (2011) 4059–4063.
[7] I. López-Corral, E. Germán, A. Juan, M.A. Volpe, G.P. Brizuela, DFT study of hydrogen adsorption on palladium decorated graphene, J. Phys. Chem. C 115 (2011) 4315–4323.
[8] H. Valencia, A. Gil, G. Frapper, Trends in the hydrogen activation and storage by adsorbed 3d transition metal atoms onto graphene and nanotube surfaces: a dft study and molecular orbital analysis, J. Phys. Chem. C 119 (2015) 5506–5522.
[9] G.M. Psofogiannakis, G.E. Froudakis, DFT Study of the hydrogen spillover mechanism on pt-doped graphite, J. Phys. Chem. C 113 (2009) 14908–14915.
[10] V. Verdinelli, E. Germán, C.R. Luna, J.M. Marchetti, M.A. Volpe, A. Juan, Theoretical study of hydrogen adsorption on Ru-decorated (8,0) single-walled carbon nanotube, J. Phys. Chem. C 118 (2014) 27672–27680.
[11] V. Tozzini, V. Pellegrini, Prospects for hydrogen storage in graphene, Phys. Chem. Chem. Phys. 15 (2013) 80–89.
[12] K. Spyrou, D. Gournis, P. Rudolf, Hydrogen storage in graphene-based materials: efforts towards enhanced hydrogen absorption, ECS J. Solid State Sci. Technol. 2 (2013) M3160–M3169.
[13] S. Gadipelli, Z.X. Guo, Graphene-based materials: synthesis and gas sorption, storage and separation, Prog. Mater. Sci. 69 (2015) 1–60.
[14] Q. Sun, Q. Wang, P. Jena, Y. Kawazoe, Clustering of Ti on a C60 surface and its effect on hydrogen storage, J. Am. Chem. Soc. 127 (2005) 14582–14583.
[15] P.O. Krasnov, F. Ding, A.K. Singh, B.I. Yakobson, Clustering of Sc on SWNT and reduction of hydrogen uptake: ab-initio all-electron calculations, J. Phys. Chem. C 111 (2007) 17977–17980.
[16] E. Beheshti, A. Nojeh, P. Servati, A first-principles study of calcium-decorated, boron-doped graphene for high capacity hydrogen storage, Carbon 49 (2011) 1561–1567.
[17] W.I. Choi, S.H. Jhi, K. Kim, Y.H. Kim, Divacancy-nitrogen-assisted transition metal dispersion and hydrogen adsorption in defective graphene: a first-principles study, Phys. Rev. B—Condens. Matter Mater. Phys. 81 (2010).
[18] P. Reunchan, S.H. Jhi, Metal-dispersed porous graphene for hydrogen storage, Appl. Phys. Lett. 98 (2011).
[19] L. Wang, K. Lee, Y.Y. Sun, M. Lucking, Z. Chen, J.J. Zhao, S.B. Zhang, Graphene oxide as an ideal substrate for hydrogen storage, ACS Nano 3 (2009) 2995–3000.
[20] G. Kim, S.H. Jhi, S. Lim, N. Park, Effect of vacancy defects in graphene on metal anchoring and hydrogen adsorption, Appl. Phys. Lett. 94 (2009).
[21] D.H. Lim, A.S. Negreira, J. Wilcox, DFT studies on the interaction of defective graphene-supported Fe and Al nanoparticles, J. Phys. Chem. C 115 (2011) 8961–8970.
[22] K.M. Fair, X.Y. Cui, L. Li, C.C. Shieh, R.K. Zheng, Z.W. Liu, B. Delley, M.J. Ford, S.P. Ringer, C. Stampfl, Hydrogen adsorption capacity of adatoms on double carbon vacancies of graphene: a trend study from first principles, Phys. Rev. B—Condens. Matter Mater. Phys. 87 (2013).
[23] S. Yadav, Z. Zhu, C.V. Singh, Defect engineering of graphene for effective hydrogen storage, Int. J. Hydrog. Energy 39 (2014) 4981–4995.
[24] A. Bhattacharya, S. Bhattacharya, C. Majumder, G.P. Das, Transition-metal decoration enhanced room-temperature hydrogen storage in a defect-modulated graphene sheet, J. Phys. Chem. C 114 (2010) 10297–10301.
[25] Z.M. Ao, Q. Jiang, R.Q. Zhang, T.T. Tan, S. Li, Al doped graphene: a promising material for hydrogen storage at room temperature, J. Appl. Phys. 105 (2009) 074307.
[26] H. Pardo, N. Divine Khan, R. Faccio, F.M. Araújo-Moreira, L. Fernández-Werner, T. Makarova, Á.W. Mombrú, Raman characterization of bulk ferromagnetic nanostructured graphite, Phys. B: Condens. Matter 407 (2012) 3206–3209.
[27] M. Terrones, A.R. Botello-Méndez, J. Campos-Delgado, F. López-Urías, Y.I. Vega-Cantú, F.J. Rodríguez-Macías, A.L. Elías, E. Muñoz-Sandoval, A.G. Cano-Márquez, J.-C. Charlier, H. Terrones, Graphene and graphite nanoribbons: morphology, properties, synthesis, defects and applications, Nano Today 5 (2010) 351–372.

[28] P. Hohenberg, W. Kohn, Inhomogeneous electron gas, Phys. Rev. 136 (1964) B864–B871.
[29] W. Kohn, L.J. Sham, Self-consistent equations including exchange and correlation effects, Phys. Rev. 140 (1965) A1133–A1138.
[30] P.E. Blöchl, Projector augmented-wave method, Phys. Rev. B 50 (1994) 17953–17979.
[31] G. Kresse, J. Furthmüller, Efficiency of ab-initio total energy calculations for metals and semiconductors using a plane-wave basis set, Comput. Mater. Sci. 6 (1996) 15–50.
[32] G. Kresse, D. Joubert, From ultrasoft pseudopotentials to the projector augmented-wave method, Phys. Rev. B—Condens. Matter Mater. Phys. 59 (1999) 1758–1775.
[33] M. Dion, H. Rydberg, E. Schröder, D.C. Langreth, B.I. Lundqvist, Van der Waals density functional for general geometries, Phys. Rev. Lett. 92 (2004) 246401.
[34] G. Román-Pérez, J.M. Soler, Efficient implementation of a van der waals density functional: application to double-wall carbon nanotubes, Phys. Rev. Lett. 103 (2009).
[35] J. Klime, D.R. Bowler, A. Michaelides, Van der Waals density functionals applied to solids, Phys. Rev. B—Condens. Matter Mater. Phys. 83 (2011).
[36] H.J. Monkhorst, J.D. Pack, Special points for Brillouin-zone integrations, Phys. Rev. B 13 (1976) 5188–5192.
[37] R. Hoffmann, Solids and Surfaces: A Chemist's View of Bonding in Extended Structures, VCH, New York, 1988.
[38] P. Ordejón, E. Artacho, J.M. Soler, Self-consistent order-N density-functional calculations for very large systems, Phys. Rev. B—Condens. Matter Mater. Phys. 53 (1996) R10441–R10444.
[39] J.M. Soler, E. Artacho, J.D. Gale, A. García, J. Junquera, P. Ordejón, D. Sánchez-Portal, The SIESTA method for ab initio order-N materials simulation, J. Phys. Condens. Matter 14 (2002) 2745–2779.
[40] J. Junquera, Ó. Paz, D. Sánchez-Portal, E. Artacho, Numerical atomic orbitals for linear-scaling calculations, Phys. Rev. B—Condens. Matter Mater. Phys. 64 (2001) 2351111–2351119.
[41] J. Wong, S. Yadav, J. Tam, C. Veer Singh, A van der Waals density functional theory comparison of metal decorated graphene systems for hydrogen adsorption, J. Appl. Phys. 115 (2014) 224301.
[42] M. Andersen, L. Hornekær, B. Hammer, Graphene on metal surfaces and its hydrogen adsorption: a meta-GGA functional study, Phys. Rev. B 86 (2012) 085405.
[43] H.-Y. Wu, X. Fan, J.-L. Kuo, W.-Q. Deng, DFT study of hydrogen storage by spillover on graphene with boron substitution, J. Phys. Chem. C 115 (2011) 9241–9249.
[44] S. Dag, Y. Ozturk, S. Ciraci, T. Yildirim, Adsorption and dissociation of hydrogen molecules on bare and functionalized carbon nanotubes, Phys. Rev. B—Condens. Matter Mater. Phys. 72 (2005) 155404.
[45] R. Faccio, L. Fernández-Werner, H. Pardo, C. Goyenola, O.N. Ventura, A.W. Mombrú, Electronic and structural distortions in graphene induced by carbon vacancies and boron doping, J. Phys. Chem. C 114 (2010) 18961–18971.
[46] P. Błoński, J. Hafner, Geometric and magnetic properties of Pt clusters supported on graphene: relativistic density-functional calculations, J. Chem. Phys. 134 (2011).
[47] A. Maiti, A. Ricca, Metal-nanotube interactions—binding energies and wetting properties, Chem. Phys. Lett. 395 (2004) 7–11.
[48] D.H. Chi, N.T. Cuong, N.A. Tuan, Y.T. Kim, H.T. Bao, T. Mitani, T. Ozaki, H. Nagao, Electronic structures of Pt clusters adsorbed on (5, 5) single wall carbon nanotube, Chem. Phys. Lett. 432 (2006) 213–217.
[49] Y. Tang, Z. Yang, X. Dai, Trapping of metal atoms in the defects on graphene, J. Chem. Phys. 135 (2011) 224704.
[50] C. Kittel, Introduction to Solid State Physics, Wiley, 2005.
[51] A.V. Krasheninnikov, P.O. Lehtinen, A.S. Foster, P. Pyykkö, R.M. Nieminen, Embedding transition-metal atoms in graphene: structure, bonding, and magnetism, Phys. Rev. Lett. 102 (2009).
[52] Y. Park, G. Kim, Y.H. Lee, Adsorption and dissociation of hydrogen molecules on a Pt atom on defective carbon nanotubes, Appl. Phys. Lett. 92 (2008).
[53] K. Momma, F. Izumi, VESTA 3 for three-dimensional visualization of crystal, volumetric and morphology data, J. Appl. Crystallogr. 44 (2011) 1272–1276.